Construction of Absolute Gravity Benchmark Offshore With an Atomic Gravimeter

Bin Wu, Yingpeng Zhao, Yin Zhou, Wenwen Yuan, Dianrong Li, Shuning Bao, Dong Zhu, Bing Cheng, Leyuan Wu, Jiangcun Zhou, Zhongkun Qiao, Xiaolong Wang, and Qiang Lin

***Abstract*—Marine gravity survey is of great significance to the fields of geophysics research, marine geological mapping, and so on. Usually, accuracy calibration is required since the gravity measurements remain relative at present. For this application, the absolute gravity reference point is necessary, which can be established with classical optical absolute gravimeters. In this article, an absolute gravity benchmark is constructed through a gravity measurement system based on a homemade atomic gravimeter at the quay of Zhoushan Archipelago. Even in the rugged environment of seaboard, a measurement sensitivity of 0.76 mGal/$\sqrt{\text{Hz}}$ is obtained. Besides, the estimated absolute accuracy of gravity is better than 30 μGal. Interestingly, it is found that the accuracy has been affected greatly by the ocean tidal loading (OTL) effect, especially the absence of an accurate OTL model in the observation region. To further investigate the OTL effect, the continuous absolute gravity observations are carried out for seven days, collecting tidal heights as well. Notably, a peak-to-peak amplitude of approximately 170 μGal is obtained even when the gravity variations caused by solid tide effect have been corrected. However, the calculated values with the existing OTL models seem much smaller than the actual gravity variation data. To solve this problem, an optimized OTL model for offshore gravity measurement has been proposed through an analysis of the existing models. With the improved model of OTL, the calculated results agree well with the experimental data. These findings offer valuable insights for the high-precision calibration of marine gravimeters.**

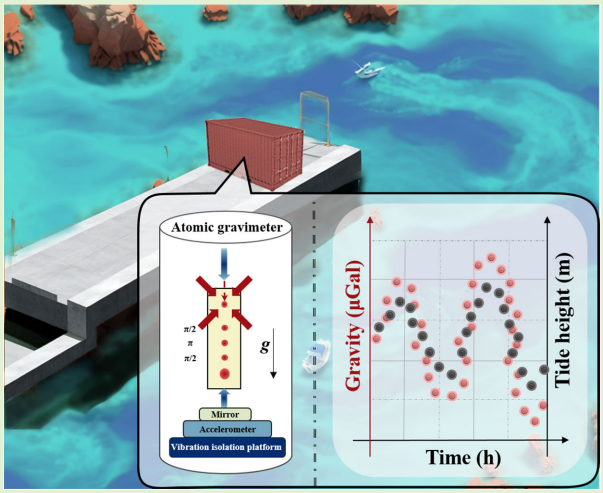

***Index Terms*— Absolute gravity, cold atomic gravimeter (CAG), ocean tidal loading (OTL).**

Manuscript received 10 May 2024; revised 29 May 2024; accepted 29 May 2024. Date of publication 10 June 2024; date of current version 1 August 2024. This work was supported in part by the National Key Research and Development Program of China under Grant 2023YFC2907000; in part by the Research and Application Experiment of Carrying Measurement and Support Technology for Ocean Route under Grant DD2021085; and in part by the National Natural Science Foundation of China (NSFC) under Grant 61727821, Grant 61475139, and Grant 11604296. The associate editor coordinating the review of this article and approving it for publication was Dr. Mert Torunbalci. *(Corresponding author: Yin Zhou.)*

Bin Wu, Yingpeng Zhao, Yin Zhou, Wenwen Yuan, Dianrong Li, Shuning Bao, Dong Zhu, Bing Cheng, Leyuan Wu, Zhongkun Qiao, Xiaolong Wang, and Qiang Lin are with Zhejiang Provincial Key Laboratory of Quantum Precision Measurement, College of Science, and the Institute for Frontier Interdisciplinary Science, Zhejiang University of Technology, Hangzhou 310023, China (e-mail: yinzhou@zjut.edu.cn; qiaozhongkun2021@zjut.edu.cn; qlin@zjut.edu.cn).

Jiangcun Zhou is with Zhejiang Provincial Key Laboratory of Quantum Precision Measurement, College of Science, and the Institute for Frontier Interdisciplinary Science, Zhejiang University of Technology, Hangzhou 310023, China, and also with the State Key Laboratory of Geodesy and Earth's Dynamics, Innovation Academy for Precision Measurement Science and Technology, Chinese Academy of Sciences, Wuhan 430071, China.

Digital Object Identifier 10.1109/JSEN.2024.3408839

I. Introduction

GRAVITY measurements are pivotal for geophysical studies, including the dynamics of subsurface fluids [1], [2], [3], marine geological mapping [4], [5], resource exploration [6], and so on. For ocean gravity measurements, they provide quantitative constraints on crustal structure and, in combination with other co-registered datasets and forward models, improve the ability to interpret the geologic processes occurring within oceanic crust. Although satellite gravity measurement can use space technology to monitor ocean gravity, the determination of satellite orbit parameters still needs to be based on surface gravity measurement data [7], [8], [9]. The gravimeters have led to a marked improvement in the quality of marine gravity [10]. Hence, the utilization of gravimeters for measuring ocean gravity remains an essential technique in the field of ocean gravity survey and marine geophysical exploration. To ensure the effectiveness of these marine gravity measurements, it is imperative to conduct periodic recalibrations and comparisons at reference points where gravity values are precisely known [11]. Consequently,

the creation of shore-based absolute gravity observation stations becomes a fundamental requirement, serving as pivotal calibration benchmarks for maintaining the accuracy and reliability of marine gravity data. (Benchmark: Establishment of shore-based absolute gravity observation points with atomic absolute gravimeter.)

Using relative gravimeters frequently encounters obstacles due to calibration inconsistencies and errors originating from instrumental drifts. Conversely, atomic absolute gravimeters present an alternative, immune to drifts and capable of executing continuous measurements over prolonged durations. This attributes that cold atomic gravimeters (CAGs) [12], [13], [14] are exceptionally suited for the establishment of shore-based gravity measurement stations. Currently, the measurement accuracy of CAGs has reached that of classical gravimeters [15]. Compared with classical gravimeters (e.g., FG-5), CAGs can achieve much higher sampling rates. Furthermore, the mobile atom gravimeters have been used for experimental validation [11], [16], [17]. For example, the AQG#B01 (former Muquans) was carried out at Larzac observatory, the repeatability to be better than 5 μGal [16], and the gravity sensitivity is 0.5 mGal/$\sqrt{\text{Hz}}$ in the field along a route of 7.6 km [17]. The internal coincidence precision is 1.22 mGal and an external coincidence accuracy is 1.62 mGal of the home-made marine survey system by Wu et al. [14]. Antoni-Micollier et al. [18] demonstrated the world's first time series acquired in the summit region of an active volcano using an absolute atomic interferometric gravimeter. As a result, the CAGs can be used in a broader range of field gravity measurements.

In coastal gravity studies, the effect of ocean tidal loading (OTL) on gravity measurements may exceed the accuracy of instruments [5], [19], necessitating corrections for OTL effects to accurately determine the absolute gravity values. Currently, tidal effects mainly include solid tides and OTL. Solid tides are relatively well-modeled with an accuracy of about 1 nGal [20]. However, the effect of OTL on gravity measurement is complex and not accurate enough because the coastal terrains are usually irregular. The resulting gravity variations by ocean tides are dominated by OTL effect [21]. In practice, the changes in gravity values due to OTL effects are more consistent with available models [22], [23], when the measurement points are located inland. However, when the gravity measurement station is located at the quay or far away from the coast, the calculation results of the current OTL model deviate more [24], [25], [26]. Therefore, in the experiment, Zhoushan sea area is selected as an ideal point for studying tidal phenomena associated with gravity measurements, and thus this point belongs to the near-shore sea area where the tidal loading effect is obvious. At present, the marine tidal load effect model of Zhoushan Islands is more analyzed [27], [28], [29], but the accuracy of gravity estimation needs to be further improved.

In this article, we established an absolute gravity reference point at Changzhi quay, Zhoushan Archipelagic, which conducted a comparison with the known reference gravity values and performed a detailed error analysis. To our knowledge, this article represents the deployment of an atomic gravimeter for shore-based gravity assessments for the first time. During our observations, we monitored variations in tide height and gravity data, identifying a significant influence of the OTL effect on the gravity measurements. This observation prompted a detailed investigation on the OTL effect, revealing discrepancies between gravity variation predicted by the existing OTL models and the actual observed gravity data. To address this issue, we optimized the traditional OTL model by incorporating the effect of regional seawater mass change. The outcomes based on this improved model showed a compelling alignment with our gravity measurement data, thereby significantly reducing the bias in calculated gravity values, particularly in regions distant from land. This improvement in the OTL model marks a pivotal advancement in minimizing errors in gravity measurements in coastal and offshore environments.

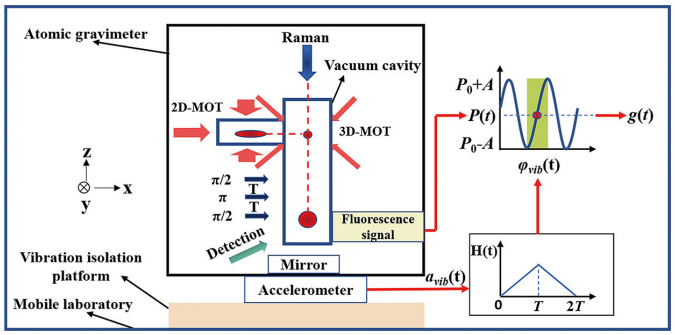

Fig. 1. Schematic of the experiment [12].

II. Experimental Setup and Experiments

A. Experimental Setup-CAG

Fig. 1 shows the entire experimental process. Due to the significant ambient vibration caused by seawater movement in shore-based or shipboard measurements, passive vibration isolation and systematic vibration compensation must be used in the measurement process. In the experiment, the vibration isolation platform uses passive vibration isolation techniques, which is used to suppress the high-frequency vibration of the environment. Accelerometers are used to measure Raman mirror vibrations to correct interference phase shifts caused by vibrations.

The gravity sensor is surrounded by a magnetic field shield with a diameter of 52 cm and height of 55 cm, and the weight of gravity sensor is about 70 kg. With the 2-D and 3-D quartz vacuum chambers, an atomic loading rate of 8×10^9/s is achieved, enabling successful trapping of ^{87}Rb for gravity measurement. In the gravity measurements, the CAG uses a precise experimental procedure that entails cooling atoms to an ultralow temperature of 4 μK before releasing them to freefall under the influence of gravity. During this freefall phase, the atoms are selected in $|F = 1, m_F = 0>$ with microwave π pulse. Subsequently, a sequence of three Raman pulses is applied to conduct atom interferometry, allowing for high-precision gravity measurements. The sequence of Raman pulses from the atomic gravimeter is $\pi/2 - \pi - \pi/2$ with a π pulse duration of 10 μs for π pulse and a time interval between adjacent Raman pulses $T = 55$ ms. The gravity value is calculated by fitting the phase of the extracted interference

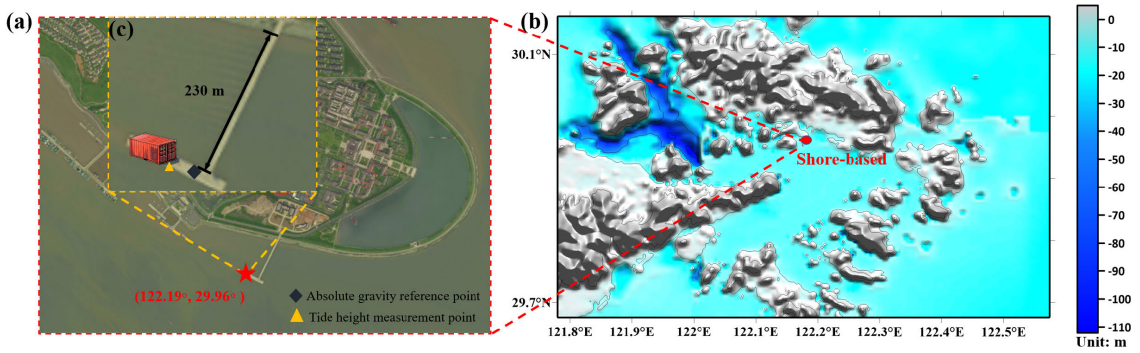

Fig. 2. Map of the measurement point in Zhoushan Archipelago area. (a) Satellite map of the region around the measurement point. (b) Elevation map around the measurement point. (c) Diagram for the position of the experimental apparatus on the quay. The red container denotes the measurement system; the black diamond displays the absolute gravity reference point, and the yellow triangle shows the point of tide height measurement.

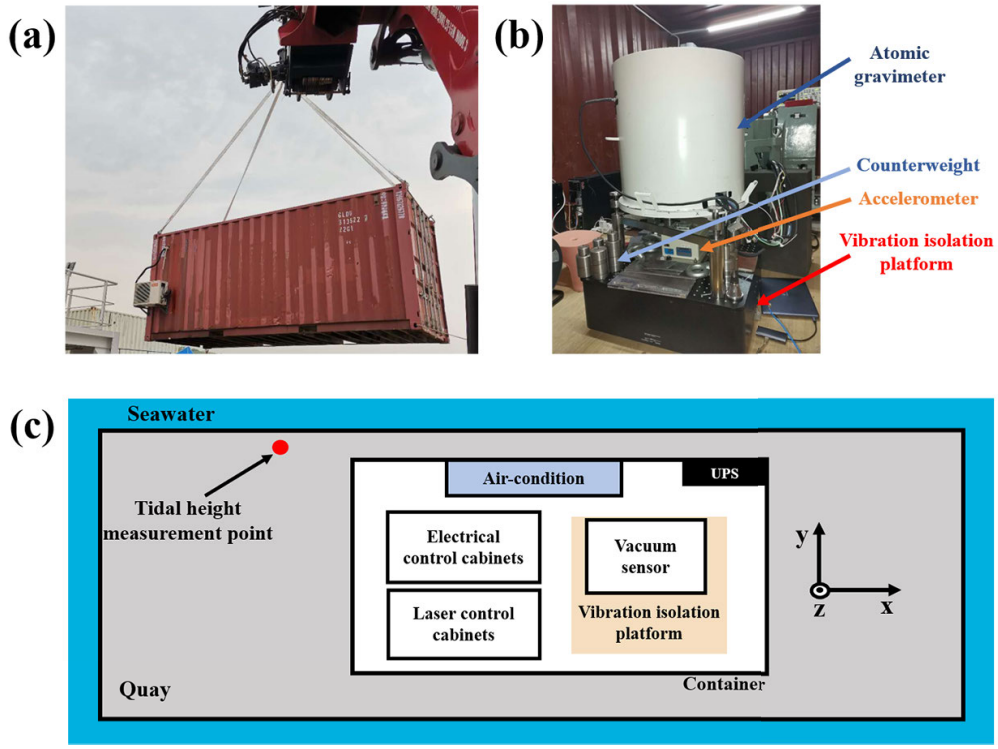

Fig. 3. Experimental devices. (a) Moveable laboratory. (b) Atomic gravimeter. (c) Layout within the mobile laboratory. Red dots denote sea surface height recording points.

fringes [12], which can be expressed as $\Delta\varphi = (\vec{\kappa}_{\text{eff}} \cdot \vec{g} - \alpha)T^2$. Where $\vec{k}_{\text{eff}}$ denotes the effective wave vector of Raman beam, α is the chirp rate of the Raman laser, and $\vec{g}$ is the gravitational acceleration. The fringe pattern, in turn, contains the gravitational acceleration information, extracted by scanning α.

B. Location of Shore-Based Measurements

In experiments, the shore base for absolute gravity measurements with an atomic gravimeter is located in the port of Zhoushan, Zhejiang, China. The shore-based measurement is approximately 230 m from the shore and is surrounded by the seawater [as shown in Fig. 2(a)]. Fig. 2(b) shows the elevation map around the observation point with the latitude and longitude indicated as (122.19°, 29.96°). There has been a relatively detailed study on modeling tidal dynamics in the vicinity of Zhoushan islands [27].

Atomic gravity measurements require attention to the environment during shore-based measurements. The most significant effects on measurements include ambient temperature and humidity, as well as vibration, which can be deteriorated by other environments. Therefore, Fig. 3(a) shows that mobile laboratory is adopted to address these issues. The atomic gravimeter, vibration isolation platform, and other instruments are placed in the mobile laboratory made of containers with dimensions 5.89 × 2.35 × 2.39 m as shown in Fig. 3(b). The shore base is located at the quay and surrounded by seawater. In the mobile laboratory, air conditioning is used to regulate the ambient temperature and ensure the optimal functioning of the laser system. In addition, an uninterruptible power supply (UPS) was used to guarantee a stable power supply for the mobile experiments. The schematic of the CAG measurement system is depicted in Fig. 3(c), illustrating the integration of three essential components: the gravity sensor

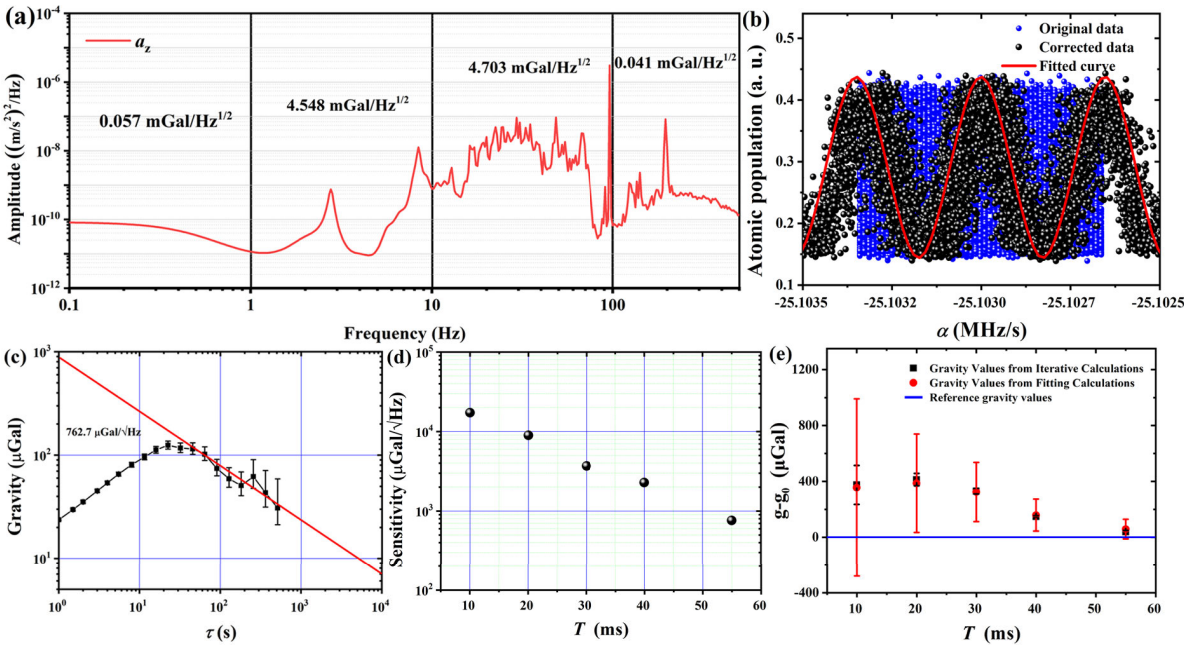

Fig. 4. Atomic gravimeter measurements at the shore base. (a) PSD of shore-based vibrations on May 30, 2020. (b) Atomic interference fringes with $T = 55$ ms. Blue dots: the original signals of atomic population; black dots: the signals after vibration correction; and red line: the fit curve. (c) Sensitivity assessment of gravity data measured on the land-based. (d) Gravity sensitivity at T of the interference pulses. (e) Gravity error at the interference pulse T. Red dots: extraction of gravity values by fitting fringes. Black dots: gravity values extracted by iterating over the interferometric phases of the atoms. Blue line: absolute gravity reference for the shore-based measurement point.

with its vibration isolation system, the optical system, and the electronic system. We record the height change in the surrounding sea at the quay, where the measurement point is located at the red dot in Fig. 3(c). For the measurement process of the atomic gravimeter, one can refer to the previous literature of our group [12]. Due to the strong effect of seawater movement on the vibration environment of the quay, the passive vibration isolation and system vibration compensation are applied during the measurement process.

III. Results

In our measurements, we used the CAG instrument with a sampling rate of 2 Hz [30]. In preparation for the gravity measurements, meticulous attention was devoted to the preliminary examination of ambient noise conditions prevailing at the dock. In addition, an in-depth investigation into the system sensitivity of the gravimeter was conducted to ensure the accuracy and reliability of our measurements.

A comprehensive systematic error analysis of the CAG instrument is detailed in [30]. The estimated noise level attributed to factors other than vibration in the system is approximately 171.3 μGal/$\sqrt{\text{Hz}}$. The primary contributors to this noise are Raman laser phase noise and detection noise. For shore-based experiments, environmental factors such as temperature and humidity have been effectively addressed through the implementation of a mobile laboratory. Consequently, the primary environmental influence on the measurements of the atomic gravimeter is vibration.

In the computation of atomic interferometric phase, it is essential to incorporate vibrational phase compensation to obtain accurate gravity values. Fig. 4(a) illustrates the power spectral density (PSD) of quay vibrations. We assessed the contribution of vibration noise to the gravity measurements to be about 13.12 mGal [31], which is the root-mean-square value calculated by integrating the transfer function of the vibration with the atomic gravimeter over a period of time. To comprehend the impact of different vibration frequency bands on the sensitivity of the gravimeter, we conducted a segmented integration of the vibration PSD. This analysis enabled the determination of the influence of each frequency band on the gravity sensitivity [as shown in Fig. 4(a)]. The impact of vibrations at different frequency intervals on the measurement sensitivity of a CAG is determined through the integration of the product of noise power spectral density of vibration and the gravimeter's transfer function. This procedure elucidates that vibration noises significantly affect the measurement sensitivity within the frequency ranges of (1, 10) Hz and (10, 100) Hz, with the estimated influences on the sensitivity of 4.548 and 4.703 mGal/$\sqrt{\text{Hz}}$, respectively. To accurately assess the effect of vibration on the sensitivity of CAG, a sum-of-squares calculation of the contributions from all the frequency intervals is required. The results indicate that the overall impact of vibrations on gravity sensitivity is approximately 6.54 mGal/$\sqrt{\text{Hz}}$, and a factor of $6.54/0.76 \approx 8.61$ is obtained with the vibration rejection system.

Therefore, the vibration data during the measurements were collected and synchronized to calculate the magnitude of the interference phase shift induced by vibrations in the atomic gravimeter at each moment. Finally, the interference fringes after vibration compensation had a fringe contrast of 31% [as shown in Fig. 4(b)]. Then, after optimizing the atomic gravimeter to the best possible state, we conducted an Allan deviation assessment of the system on May 30, 2020. (The detailed introduction of this method could be found in [32], [33], and [34].) Fig. 4(c) shows the Allan deviation of the measured gravity data at $T = 55$ ms, which is 0.76 mGal/$\sqrt{\text{Hz}}$.

The gravity sensitivity is evaluated for different pulse intervals T [as shown in Fig. 4(d)]. According to the results, the sensitivity of atomic gravimeter improves as T increases.

Before the experiment, the errors in gravity measurement with different interference pulse durations (T) were analyzed, and each measurement took approximately 1 h. Fig. 4(e) illustrates the measurement results. Two gravity extraction methods were compared during the tests: 1) the method based on fringe fitting (red dots) and 2) the interferometric phase iteration method used in this article (black) [12], [35]. The results indicate that for an interference pulse length of $T =$ 55 ms, the measurement standard deviation with fringe fitting is 70 μGal, while the standard deviation of the iterative method used in this article is 12 μGal [Type A uncertainty (Δ_A)]. Type B uncertainty primarily includes uncertainties related to the correction of the CAG system and external environmental parameters. Specifically, the uncertainties associated with the correction of the atomic gravimeter system involve factors such as two-photon light shift, Coriolis force, and Raman beam wavefront. For the atomic gravimeter used in this study, the uncertainty associated with systematic effect corrections is approximately 10 μGal. Detailed assessments can be found in previously published articles by the research group [12], [30], [36]. Furthermore, a comparison was made between the gravity reference value provided by the shore base and the gravity values measured by the atomic gravimeter, with a deviation of about 70.48 μGal being observed.

Hence, the combined uncertainty of the dynamic gravimetric measurements at the benchmark $\Delta_{\text{quay}} = (\Delta_A^2 + \Delta_B^2)^{1/2}$ is about 15.62 μGal. The measurement uncertainty (Δ_{rf}) of the absolute gravity reference point is 30 μGal. Therefore, the final uncertainty ($\Delta = (\Delta_{\text{quay}}^2 + \Delta_{\text{rf}}^2)^{1/2}$) is about 33.82 μGal. The final comparison measurement with the absolute gravity value of the shore base is (70.48 $\pm$ 33.82) μGal. Moreover, the error is less than 300 μGal, satisfying the benchmark specifications for marine gravity measurements in China.

From the results, the main source of error arises from environmental vibrations, and it is possible that the system state may not have been optimized to its best. However, upon excluding systematic effects from the measured absolute gravity values, we observed a persistent periodic deviation with a period of about 12 h. Therefore, we suspect that this phenomenon may be attributed to the tidal loading effect.

During our week-long gravity observation experiment conducted at the quay with atomic gravimeter, we have specifically concentrated our analysis on the gravity data acquired between June 3 and June 6, 2020. This particular timeframe was chosen due to its notably enhanced data completeness. In processing the gravity data, the usual corrections are made to atomic gravimeter to avoid the influence of nontidal factors, such as systematic error correction, Coriolis force correction, latitude correction, and solid tide correction.

Fig. 5 shows the relationship between gravity values, height variations in ocean tides, and measurement time. Gravity measurement was performed for a period of 61 h. We have observed a correlation between variations in tidal height and changes in gravity values. Analysis indicates that the primary cause of gravity fluctuations is attributed to the tidal loading

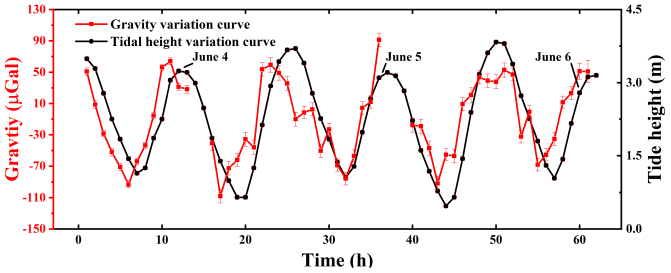

Fig. 5. Variations in gravity values and tide heights with time (time: 3 June, 1 pm–6 June, 1 am).

effect. The peak-to-peak variation in gravity values can reach up to 170 μGal. Furthermore, there is an approximate 3-m variation in tidal height. Upon consulting literature on tidal loading, using the existing tidal loading models yields a maximum gravity variation of approximately 40 μGal. Our results reveal that the estimated gravity changes from the existing tidal loading models are approximately four times smaller than the actual measured values. Consequently, we conducted an in-depth analysis to investigate the impact of tidal loading models on gravity measurements.

IV. Discussion

To elucidate the discrepancies in tidal load calculations produced by different models, we selected two widely used models alongside our enhanced tidal load model for comparative analysis. The prevalent models in current use include Green's integral model (NAO99) and the spherical harmonic function model (FES2014), each with its distinct computational frameworks and accuracy determinants, which will be elaborated upon subsequently. The spherical harmonic model is an approximation of the solution, which bases its accuracy on the function's order. The accuracy of Green's function integral model hinges on several factors: the resolution of the tidal grid, the delineation ambiguity between sea and land within the grid, and the computational precision of tidal integrals.

In response, our improvements focused on refining Green's integral approach. We segmented the OTL model into global and local components, conducting calculations for each segment individually. For the global tidal loading influence, we applied Green's integral to exclude the local area's effect. Subsequently, we recalculated the changes in seawater mass within the local region with Green's equation. The results of these calculations represent the gravity change at the observation point induced by OTL effect, which offers a novel understanding of OTL effects.

A. Variation in Gravity Due to Global Ocean Tides

The prevalent methods for enhancing the precision of the OTL effect [24] calculations typically involve the application of the near-Earth Green's integral algorithm. The calculation encompasses two components: the direct effect (Newtonian effect) and the indirect effect (elastic effect). The effect of tidal loading on gravity can be expressed as [37]

$$\Delta g_{\text{global}}(\phi_p, \lambda_p) = G\rho_w \int\int_{D-\bar{D}} h_q G_i(\psi_{pq}) d\sigma_q + G\rho_w \int\int_{D-\bar{D}} h_q G_d(\psi_{pq}) d\sigma_q \quad (1)$$

where p is the gravity observation base point, and q is the ocean tidal height of measurement point, ϕ_p and λ_p, respectively, are the latitude and longitude of p, D is the entire domain of a spherical Earth, $\bar{D}$ is the local domain of observation point, G is the gravitational constant, ρ_w is the density of water, h_q is the tidal height above the local mean sea surface, ψ_{pq} is the spherical angle between the gravimetric shore-based p and the ocean tide point $q(\phi_q, \lambda_q)$, and σ_q is the unit area of the region $D(d\sigma_q = \cos\phi_q d\phi_q d\lambda_q)$. Green's functions, namely, $G_i(\psi_{pq})$ for the indirect load effect and $G_d(\psi_{pq})$ for the direct load effect, can be derived as follows:

$$\begin{cases} G_i(\psi_{pq}) = -\dfrac{\bar{g}}{M}\left(\dfrac{k'_\infty - 2h'_\infty}{2\sin(\psi_{pq}/2)} - \displaystyle\sum_{n=0}^{\infty}\left[(n+1)k'_n - k'_\infty \right.\right. \\ \qquad\qquad \left.\left. -2\left(h'_n - h'_\infty\right)\right]P_n(\cos\psi_{pq})\right) \\ G_d(\psi_{pq}) = \dfrac{\gamma}{M}\dfrac{1}{4\sin(\psi_{pq}/2)} \end{cases} \tag{2}$$

where $\bar{g}$ is the Earth's gravitational constant ($\bar{g} \approx 9.81$ m/s^2), M is the mass of the Earth, h'_n and k'_n are the load Love numbers for n degrees [38], [39], h'_∞ and k'_∞ are the load Love numbers for the infinite degrees, γ is the quality factor [37], and P_n is the Legendre polynomials. The tidal load's gravitational effect at the measurement point p can be computed by integrating Green's function of the near-surface tidal load effect. This process is facilitated by the NAO99 model [40], [41], [42], encompassing nine subtidal components (K1, K2, M2, N2, O1, P1, Q1, S2, and Mf) with a tidal grid model resolution of 0.5° × 0.5°. The model covers a regional latitude and longitude range from 0° to 180° and 0° to 360°, respectively.

As a comparison, a spherical harmonic coefficient model was chosen to calculate the tidal load of the observed site tides [43]. The equivalent water height variation h_q at the q points (r_q, ϕ_q, and λ_q) can be expressed as the number of spherical harmonic steps of the speciated load as follows:

$$\bar{h}_q(\phi_q, \lambda_q) = R_e \sum_{n=1}^{\infty}\sum_{m=0}^{n}[\Delta C^w_{nm}\cos m\lambda + \Delta S^w_{nm}\sin m\lambda]\,\bar{P}_{nm}(\cos\theta) \tag{3}$$

where R_e is the mean radius of the Earth, ΔC^w_{nm}, ΔS^w_{nm} is the nth-order m-specified load spherical harmonic coefficient, and $\bar{P}_{nm}$ is the fully normalized associated Legendre functions [44]. ΔC^w_{nm}, ΔS^w_{nm} for a fully specified change in the bit coefficient can be expressed as

$$\begin{aligned} \Delta\bar{C}_{nm} &= \frac{4\pi {R_e}^3}{M}\frac{\rho_w}{2n+1} \\ \Delta C^w_{nm} &= \frac{3}{2n+1}\frac{\rho_w}{\rho_q}\Delta C^w_{nm} \\ \Delta\bar{S}_{nm} &= \frac{3}{2n+1}\frac{\rho_w}{\rho_e}\Delta S^w_{nm} \end{aligned} \tag{4}$$

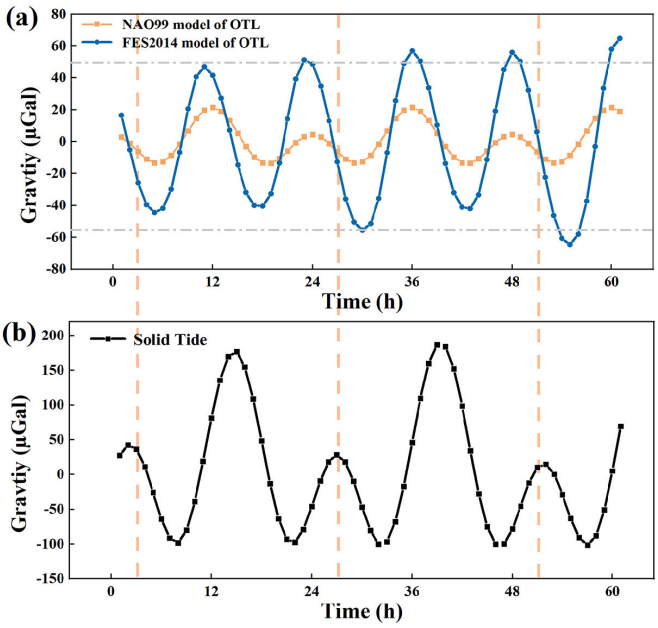

Fig. 6. Effect of tides on gravity (time: 3 June, 1 pm–6 June, 1 am). (a) Gravity values change due to the OTL effect. (b) Gravity values change due to the solid tide on gravity.

where ρ_e is the average density of the Earth and M is the total mass. The gravity load effect at observation point p can be expressed as

$$\Delta g_{\text{Spherical}}(\phi_p, \lambda_p) = \frac{GM}{{R_e}^2}\sum_{n=2}^{\infty}(n+1)\left(\frac{a}{R_e}\right)^n \times\left(1 + \frac{2}{n}h'_n - \frac{n+1}{n}k'_n\right) \sum_{m=0}^{n}(\Delta\bar{C}_{nm}\cos m\lambda_p + \Delta\bar{S}_{nm}\sin m\lambda_p)\bar{P}_{nm}(\cos\phi_p) \tag{5}$$

where a is the mean radius of the Earth. In the calculation, the degree "n" is set to 180. For the OTL calculations, the FES2014 global model can be selected [45]. FES2014 contains spherical harmonic coefficients for tidal height for 36 subtides (Ω1, Ω2, 2N2, Eps2, J1, K1, K2, L2, La2, M2, M3, M4, M6, M8, Mf, MKS2, Mm, MN4, MS4, MSf, MSqm, Mtm, Mu2, N2, N4, Nu2, O1, P1, Q1, R2, S1, S2, S4, Sa, and Ssa, T2) and the 360th-order spherical harmonic coefficient in the ETideLoad 4.5 program.

We have theoretically computed the variation in gravity induced by the OTL effect at the Zhoushan quay [as shown in Fig. 6(a)]. The orange dotted line in the graph represents the gravity fluctuations as a result of the tides, calculated with NA099 model. In addition, for comparison, we have also depicted gravity variations (the blue dotted line) calculated with the global FES2014 model. In addition, to compare the solid tide with the OTL effect, we calculate the change in gravity values due to solid tide based on ETERNA34 [20], [46] at the quay [as shown in Fig. 6(b)]. The change in gravity values due to the OTL effect of the ocean tides is relatively small compared with the solid tide. To better analyze the effect of ocean tides on gravity, we first correct for the solid tide in data processing.

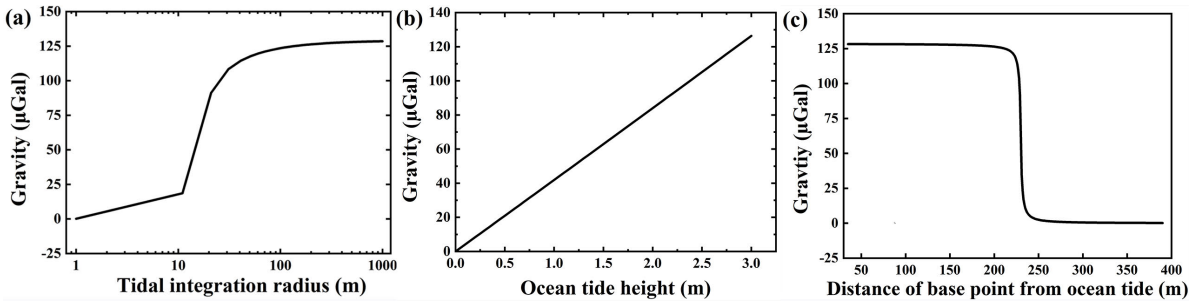

Fig. 7. Theoretical calculation of gravity variations due to tidal mass. (a) Effect of integration radius of measured area on calculated gravity. (b) Effect of height of tide on gravity. (c) Variation in gravity values with distance from the center of the tide to the observation point.

B. Variation of gravity Due to Local Ocean Tides

The local seawater loading effect mainly considers the mass of seawater on the gravitational influence of measurement station, and the elasticity effect of the measurement point near the sea can be ignored. In the calculation, we equate the seawater in the area of the measurement point to a cylinder of volume $\bar{V}$. For the effect caused by the seawater mass in the region, we can use the basic geometric model to calculate the gravity changes [47], [48]. The gravity due to a 3-D body with density $\rho_w(\xi, \eta, \zeta)$ and arbitrary shape observed at point (x, y, z) is

$$\Delta g_{\text{local}}(x, y, z) = -G \iiint_{\bar{V}} \rho_w(\xi, \eta, \zeta) \frac{z - \zeta}{r^3} d\xi d\eta d\zeta$$
$$r = \sqrt{(x - \xi)^2 + (y - \eta)^2 + (z - \xi)^2}. \quad (6)$$

The unit volume change in seawater due to the movement of the tide near the measurement point can be approximated as a cylinder. Therefore, we analyze the change in gravity values due to the tidal height. In the calculation, the integration area of seawater and the tidal height have an effect on gravity. To evaluate the effect of both the factors on gravity, we take the observation point at a distance of 230 m. (The measurement point is about 230 m away from the shore.) The influence of the tidal integration radius on the gravity value of observation point at a tidal height of 3 m [as shown in Fig. 7(a)] and the influence of tidal height on the gravity value of observation point at an integration radius of 230 m are calculated [as shown in Fig. 7(b)]. In addition, we calculate a curve of distance between the center of tide and the observation point versus the value of gravity when the integration radius is 230 m, and the tidal height is 3 m [as shown in Fig. 7(c)]. It can be observed that the change in the mass of seawater caused by tide has a significant effect on gravity values when the observation point is located at the center of tide.

The total change in gravity values at the shore base can be written as

$$\Delta g_{\text{total}} = \Delta g_{\text{global}}(\phi_p, \lambda_p) + \Delta g_{\text{local}}(x, y, z). \quad (7)$$

C. Analysis of Results

For the tidal height variations at the quay, we performed theoretical calculations based on the FES2014 model with the global tidal load spherical harmonic function [as shown in Fig. 8(a)]. The black dashed line indicates the change in ocean tidal height versus the time of measurement, and the gray dashed line indicates the change in ocean tidal height as

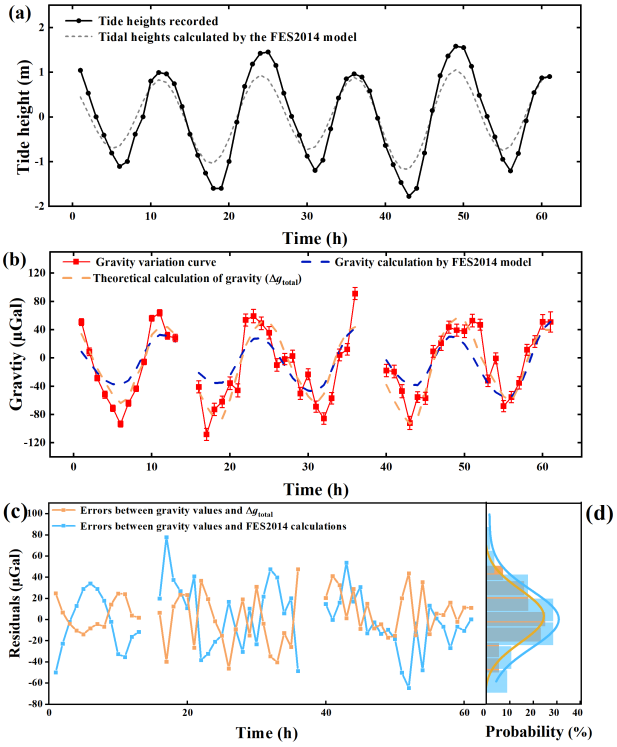

Fig. 8. Comparison between the recorded data and the models. (a) Tide height measurements versus theoretical calculations. (b) Theoretical gravity values and actual gravity values. (c) Residuals between the theoretical and actual values of gravity. (d) Distribution of residuals. The orange line is Δg_{total} residuals fit with a normal distribution. The blue line is residuals of the FES2014 model fit with a normal distribution.

calculated by FES2014. By comparison, it was found that the theoretical of tide height variation is almost identical in phase with the actual variation. However, the calculated variation in the height of tides is smaller than the actual.

Then, we compare the actual gravity data at the shore base with the theoretical data [as shown in Fig. 8(b)]. The red curve represents the actual measured change in gravity, The black curve represents the measured gravity variation, the blue dashed line represents the theoretical gravity values calculated based on the FES2014 model; and the orange dashed line represents the theoretically calculated gravity values, which include the gravity variation due to global tidal loading and regional seawater mass change. The commonly applied FSE2014 model based on the spherical harmonic approach to calculate the OTL effect was found to be small in the results. In comparison, the global tidal load effect is calculated with

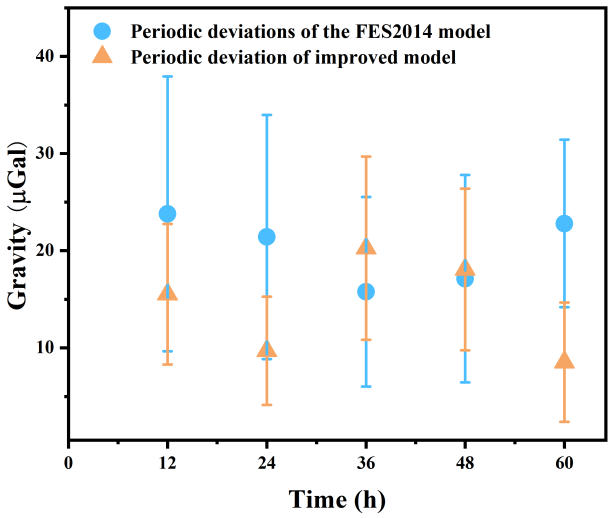

Fig. 9. Periodic deviation with a period of about 12 h between the model calculations and the observed gravity data.

Green's integral method, which takes into account the mass change in the regional tide in addition to the area of the measurement point.

Finally, we carry out an error analysis of the residuals [as shown in Fig. 8(c)]. The blue dotted line is the error between the actual gravity value and the calculation result based on the FES2014 tide model; the orange dotted line is the error between the actual gravity values and the gravity calculation considering the local tide correction. Fig. 8(d) shows the histogram of the residuals. Through theoretical analysis, the error signals for atomic gravimeters mainly comprise long-periodic variations caused by the Earth's tides, crustal movements, etc. and random errors (Gaussian distributions) in the measurements. To eliminate the influence of other errors, we have made gravity corrections for tides, Coriolis force, etc., and the remaining measurement error should be closer to the random error. By comparing the two methods, it is found that the error distribution between the calculation results based on the FES2014 tide model and the actual gravity value is wider, and the standard deviation of the error is 29.29 μGal. However, the results calculated from the global OTL Green's integral and corrected for the mass of local seawater are closer to the actual gravity values, and the standard deviation of the error is 21.96 μGal.

Fig. 9 illustrates the periodic discrepancies between the calculated outcomes of various models and the actual observed gravity data. Over a span of 61 h, including four cycles with each cycle lasting 12 h, we determined the average deviation for these 12-h intervals (taking the absolute value of the error) and calculated the corresponding error bars (the standard deviation) for each period. A comparative analysis of the bias results from both the approaches reveals that the bias associated with the refined tidal load model is notably smaller than that observed with the FES2014 model, with the error bars for the improved model consistently smaller as well. Furthermore, the bias due to periodicity leans toward random errors, exhibiting no significant periodic pattern.

V. Conclusion

The objective of this study was to investigate the effect of tidal loading on shore-based gravity measurements with the CAG, particularly in regions far from the coastline. In our experiments, we successfully mitigated the impact of environmental factors on gravity measurements and conducted continuous gravity observations at a quay reference point with the CAG. Furthermore, we recorded tidal height variations on the shore about 1 m away from the gravity measurement point. Our measurements revealed that CAG exhibited good stability with a sensitivity of approximately 0.76 mGal/$\sqrt{\text{Hz}}$. Moreover, the absolute gravity value measured at the shore base against the reference gravity value is (70.48 $\pm$ 33.82) μGal. Through a comparative analysis of our measurement results and calculations based on the existing tidal loading models, we identified potential discrepancies in the results obtained from current tidal loading models. To address inaccuracies in gravity calculations resulting from OTL effects in coastal gravity measurements far from the shore, we improved the tidal loading models. In our experiments, we observed that incorporating local seawater height variations into the model and separately calculating the impact of global tidal loading and regional seawater mass changes significantly enhanced the model's calculation accuracy. Ultimately, our theoretical values were compared with actual data, revealing that tidal loading models considering local tidal variations were more reliable. The actual change in gravity due to ocean tide loading is about 170 μGal, and the residual after model correction is 21.96 μGal, which has a coefficient of improvement by a factor of 0.75 (ratio value of standard deviation from two models) with respect to the conventional model of ocean tide loading (FES2014). Hence, this research holds substantial significance in enhancing the precision of absolute oceanic gravity measurements and refining the measurement accuracy of reference points for shipborne gravity surveys within the academic domain.

Acknowledgment

The authors express gratitude to their colleagues for the assistance provided during the experimental measurements. Special thanks are extended to Dr. Peijun Chen and Dr. Shuping Peng for their dedicated maintenance of the isolation platform, as well as to Li Chu for ensuring the operational support at the experimental site.

References

[1] D. Chapman, E. Sahm, and P. Gettings, "Monitoring aquifer recharge using repeated high-precision gravity measurements: A pilot study in South Weber, Utah," *Geophysics*, vol. 73, no. 6, pp. WA83–WA93, 2008.

[2] E. Gasperikova and G. Hoversten, "Gravity monitoring of CO_2 movement during sequestration: Model studies," *Geophysics*, vol. 73, no. 6, pp. WA105–WA112, 2008.

[3] F. Greco, G. Currenti, R. Napoli, A. Pistorio, and C. Del Negro, "Combining relative and absolute gravity measurements to enhance volcano monitoring," *Bull. Volcanol.*, vol. 74, pp. 1745–1756, 2012.

[4] Y. Bai, S. E. Williams, R. D. Müller, Z. Liu, and M. Hosseinpour, "Mapping crustal thickness using marine gravity data: Methods and uncertainties," *Geophysics*, vol. 79, no. 2, pp. G27–G36, Mar. 2014.

[5] A. Watlet et al., "Gravity monitoring of underground flash flood events to study their impact on groundwater recharge and the distribution of Karst voids," *Water Resour. Res.*, vol. 56, no. 4, Apr. 2020, Art. no. e2019WR026673.

[6] D. Difrancesco, "Advances and challenges in the development and deployment of gravity gradiometer systems," in *Proc. EGM Int. Workshop*, 2007, p. 166.

[7] M. Lequentrec-Lalancette, C. Salaűn, S. Bonvalot, D. Rouxel, and S. Bruinsma, "Exploitation of marine gravity measurements of the Mediterranean in the validation of global gravity field models," in *Proc. Int. Symp. Earth Environ. Sci. Future Generat. IAG Gen. Assem.*, Prague, Czech Republic. Cham, Switzerland: Springer, 2015, pp. 63–67.

[8] O. Andersen, P. Knudsen, and L. Stenseng, "The DTU13 MSS (mean sea surface) and MDT (mean dynamic topography) from 20 years of satellite altimetry," in *Proc. 3rd Int. Gravity Field Service (IGFS)*, Shanghai, China. Cham, Switzerland: Springer, Jul. 2014, pp. 111–121.

[9] J. D. Fairhead, C. M. Green, and M. E. Odegard, "Satellite-derived gravity having an impact on marine exploration," *Lead. Edge*, vol. 20, no. 8, pp. 873–876, 2001.

[10] M. N. Nabighian et al., "Historical development of the gravity method in exploration," *Geophysics*, vol. 70, no. 6, p. 63, 2005.

[11] Y. Bidel et al., "Absolute marine gravimetry with matter-wave interferometry," *Nature Commun.*, vol. 9, no. 1, p. 627, Feb. 2018.

[12] C. Bing et al., "Absolute gravity measurement based on atomic gravimeter under mooring state of a ship," *Acta Phys. Sinica*, vol. 70, no. 4, 2021, Art. no. 040304.

[13] R. Geiger et al., "Detecting inertial effects with airborne matter-wave interferometry," *Nature Commun.*, vol. 2, no. 1, p. 474, Sep. 2011.

[14] B. Wu, "Marine absolute gravity field surveys based on cold atomic gravimeter," *IEEE Sensors J.*, vol. 23, no. 20, pp. 24292–24299, Oct. 2023.

[15] H. J. McGuinness, A. V. Rakholia, and G. W. Biedermann, "High data-rate atom interferometer for measuring acceleration," *Appl. Phys. Lett.*, vol. 100, no. 1, 2012, Art. no. 011106.

[16] A.-K. Cooke, C. Champollion, and N. L. Moigne, "First evaluation of an absolute quantum gravimeter (AQG# b01) for future field experiments," *Geosci. Instrum., Methods Data Syst.*, vol. 10, no. 1, pp. 65–79, 2021.

[17] X. Wu et al., "Gravity surveys using a mobile atom interferometer," *Sci. Adv.*, vol. 5, no. 9, 2019, Art. no. eaax0800.

[18] L. Antoni-Micollier et al., "Detecting volcano-related underground mass changes with a quantum gravimeter," *Geophys. Res. Lett.*, vol. 49, no. 13, 2022, Art. no. e2022GL097814.

[19] K. Naganawa et al., "Updated absolute gravity rate of change associated with glacial isostatic adjustment in Southeast Alaska and its utilization for rheological parameter estimation," *Earth, Planets Space*, vol. 74, no. 1, pp. 1–27, 2022.

[20] K. Schueller, "Theoretical basis for Earth Tide analysis with the new ETERNA34-ANA-V4. 0 program," *Bull. Inf. Marées Terrestres*, vol. 149, no. 12, pp. 12–24, 2015.

[21] M. Hendershott, "The effects of solid earth deformation on global ocean tides," *Geophys. J. Int.*, vol. 29, no. 4, pp. 389–402, 1972.

[22] H. Zhao et al., "Combining the tide gauge stations and GPS/GLONASS observations to validate global and regional ocean tide models around China coast," *J. Surveying Eng.*, vol. 148, no. 3, Aug. 2022, Art. no. 04022004.

[23] H. Tan et al., "Evaluation of global ocean tide models based on tidal gravity observations in China," *Geodesy Geodynamics*, vol. 12, no. 6, pp. 451–458, 2021.

[24] C. Hwang and J.-F. Huang, "SGOTL: A computer program for modeling high-resolution, height-dependent gravity effect of ocean tide loading," *Terr., Atmos. Ocean. Sci.*, vol. 23, no. 2, pp. 1–11, 2012.

[25] K. Matsumoto, T. Sato, T. Takanezawa, and M. Ooe, "GOTIC2: A program for computation of oceanic tidal loading effect," *J. Geodetic Soc. Jpn.*, vol. 47, no. 1, pp. 243–248, 2001.

[26] P. Mazzega, "The M2 oceanic tide recovered from Seasat altimetry in the Indian Ocean," *Nature*, vol. 302, no. 5908, pp. 514–516, 5908.

[27] Y. Zha, L. Li, L. Zhang, and Y. Xia, "Study on characteristics of tidal dynamics and vortex in Zhoushan Archipelago sea area," *IOP Conf. Ser., Earth Environ. Sci.*, vol. 725, no. 1, 2021, Art. no. 012001.

[28] D. Song, K. Cheng, B. Li, X. Xu, L. Deng, and C. Liu, "Estimation of tidal current asymmetry in an archipelagic region: The Zhoushan islands," *Water*, vol. 14, no. 9, p. 1485, 2022.

[29] J. Arnoso, M. Bos, M. Benavent, N. Penna, and E. Vélez, "OTl calculations for studying the elastic response of the upper crust in Gran Canaria (Canary Archipelago)," *Differences*, vol. 2, no. 1, p. 1, 2013.

[30] D. Zhu et al., "Metrological traceability method for atomic absolute gravimeters," *Appl. Opt.*, vol. 60, no. 26, pp. 7910–7920, 2021.

[31] J. Guo et al., "Vibration compensation for a vehicle-mounted atom gravimeter," *IEEE Sensors J.*, vol. 22, no. 13, pp. 12939–12946, Jul. 2022.

[32] A. Peters, K. Y. Chung, and S. Chu, "High-precision gravity measurements using atom interferometry," *Metrologia*, vol. 38, no. 1, p. 25, 2001.

[33] J. Le Gouët et al., "Limits to the sensitivity of a low noise compact atomic gravimeter," *Appl. Phys. B, Lasers Opt.*, vol. 92, no. 2, pp. 133–144, Aug. 2008.

[34] B. Wu, Z. Wang, B. Cheng, Q. Wang, A. Xu, and Q. Lin, "The investigation of a μGal-level cold atom gravimeter for field applications," *Metrologia*, vol. 51, no. 5, p. 452, 2014.

[35] Y. Zhou et al., "A testing method for shipborne atomic gravimeter based on the modulated Coriolis effect," *Sensors*, vol. 23, no. 2, p. 881, 2023. [Online]. Available: https://www.mdpi.com/1424-8220/23/2/881

[36] W. Bin et al., "Static measurement of absolute gravity in truck based on atomic gravimeter," *Acta Phys. Sinica*, vol. 69, no. 6, pp. 1–8, 2020, Art. no. 060302, doi: 10.7498/aps.69.20191765.

[37] W. Farrell, "Deformation of the Earth by surface loads," *Rev. Geophys.*, vol. 10, no. 3, pp. 761–797, Aug. 1972.

[38] J. Y. Guo, "Direct proof of the asymptotic expression of the loading love numbers," *Chin. J. Geophys.*, vol. 43, no. 4, pp. 549–555, 2000.

[39] S. H. Na and J. Baek, "Computation of the load love number and the load green's function for an elastic and spherically symmetric earth," *J. Korean Phys. Soc.*, vol. 58, no. 5, pp. 1195–1205, 2011.

[40] X. Lelin, L. Hui, X. Songbai, K. Kaixuan, and L. Xiaoling, "Long-term gravity changes in Chinese Mainland from grace and ground-based gravity measurements," *Geodesy Geodynamics*, vol. 2, no. 3, pp. 61–70, 2011.

[41] S. Lambotte, L. Rivera, and J. Hinderer, "Vertical and horizontal seismometric observations of tides," *J. Geodynamics*, vol. 41, nos. 1–3, pp. 39–58, 2006.

[42] T. F. Baker and M. S. Bos, "Tidal gravity observations and ocean tide models," *J. Geodetic Soc. Jpn.*, vol. 47, no. 1, pp. 76–81, 2001.

[43] F. Lyard, F. Lefevre, T. Letellier, and O. Francis, "Modelling the global ocean tides: Modern insights from FES2004," *Ocean Dyn.*, vol. 56, nos. 5–6, pp. 394–415, Sep. 2006.

[44] A. M. Dziewonski and D. L. Anderson, "Preliminary reference earth model," *Phys. Earth Planet. in.*, vol. 25, no. 4, pp. 297–356, Jun. 1981.

[45] M. A. King and L. Padman, "Accuracy assessment of ocean tide models around Antarctica," *Geophys. Res. Lett.*, vol. 32, no. 23, 2005, Art. no. L23608.

[46] H. Wenzel, *Earth Tide Data Processing Package ETERNA Version 3.40 Manual ETERNA34*. Karlsruhe, Germany: HLP. Black Forest Observatory Universität Karlsruhe, 1997.

[47] R. A. Werner and D. J. Scheeres, "Exterior gravitation of a polyhedron derived and compared with harmonic and mascon gravitation representations of asteroid 4769 Castalia," *Celestial Mech. Dyn. Astron.*, vol. 65, no. 3, pp. 313–344, 4769.

[48] X. Li and M. Chouteau, "Three-dimensional gravity modeling in all space," *Surv. Geophys.*, vol. 19, no. 4, pp. 339–368, 1998.

Bin Wu received the Ph.D. degree in optics from the Department of Physics, Zhejiang University, Hangzhou, China, in 2014.

In 2012, he went to LNE-SYRTE, Paris, France, on a joint training program to conduct research on atomic gravimeter. After the Ph.D. degree, he joined the Faculty of Science, Zhejiang University of Technology, Hangzhou, where he is currently an Associate Professor with the Department of Applied Physics, working on quantum precision measurement science and technology, quantum optics, cold atomic physics, atomic interferometry, and quantum gravimetry.

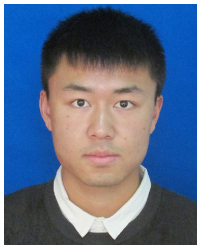

Yingpeng Zhao is pursuing the Ph.D. degree with the School of Science, Zhejiang University of Technology, Hangzhou, China.

His research interests include the fields of cold atom interferometry, quantum precision measurement, and diffraction measurement.

Yin Zhou received the B.S. degree in microelectronics from Jilin University, Changchun, China, in 2014, and the Ph.D. degree in control science and engineering from Zhejiang University of Technology, Hangzhou, China, in 2020.

He is currently a Postdoctoral Researcher with Zhejiang University of Technology. His research interests include atom interferometry and precision absolute gravity measurement.

Wenwen Yuan is pursuing the master's degree with the School of Science, Zhejiang University of Technology, Hangzhou, China.

Her research interests include quantum precision measurement.

Dianrong Li is pursuing the Ph.D. degree with the College of Science, Zhejiang University of Technology, Hangzhou, China.

Her research interests include cold atomic gravity measurement and quantum optics.

Shuning Bao is pursuing the master's degree with the College of Science, Zhejiang University of Technology, Hangzhou, China.

Her research interests include quantum precision measurement and gravity and geomagnetic data processing.

Dong Zhu received the Ph.D. degree from the College of Information Engineering, Zhejiang University of Technology, Hangzhou, China, in 2022.

He is a Postdoctoral Researcher with the College of Science, Zhejiang University of Technology. His research interests include cold atomic gravimeter, dynamic absolute gravimeter, and data processing.

Bing Cheng received the Ph.D. degree in optics from Zhejiang University, Hangzhou, China, in 2013, and the Ph.D. degree from Paris Observatory, Paris, France, in 2016.

His research interests include technical areas including laser transmission, laser frequency control, laser cooling principles, atom–laser interactions, and atomic interference.

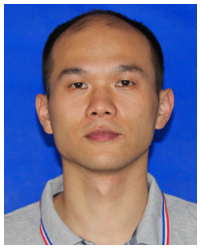

Leyuan Wu received the B.S. degree in geographic information system and the Ph.D. degree in geophysics from Zhejiang University, Hangzhou, China, in 2009 and 2014, respectively.

He is currently a Lecturer with Zhejiang University of Technology, Hangzhou. His current research interests include modeling and inversion of geophysical gravity and magnetic field, and their application to environmental and resource-exploration problems.

Jiangcun Zhou received the Ph.D. degree in geophysics from the University of Chinese Academy of Sciences, Beijing, China, in 2008.

He is currently a Researcher with the State Key Laboratory of Geodesy and Earth's Dynamics, Innovation Academy for Precision Measurement Science and Technology, Chinese Academy of Sciences, Wuhan, China, working on deformation of the Earth due to different source origins, such as tide generating force, ocean tide loading, and earthquakes.

Zhongkun Qiao received the Ph.D. degree from the College of Earth Exploration Science and Technology, Jilin University, Changchun, China, in 2021.

He is a Lecturer with the Institute for Frontiers and Interdisciplinary Sciences, Zhejiang University of Technology, Hangzhou, China. His research interests include research and application of geophysical exploration technology in aviation and ocean.

Xiaolong Wang received the Ph.D. degree in optics from the Department of Physics, Zhejiang University, Hangzhou, China, in 2011, and the Ph.D. degree in physics from Paris Observatory, Paris, France, in 2011.

His research interests include atom interferometry, spectroscopy, spectroscopic instruments, and optics and laser physics.

Qiang Lin received the Ph.D. degree in science from Zhejiang University, Hangzhou, China, in 2003.

He has long been engaged in the research of quantum precision measurement, quantum optics, and laser physics, including developing high-precision quantum gravimeter and quantum magnetometer and their applications.

Dr. Lin was a recipient of the National Natural Science Foundation of China Distinguished Youth Fund and German Humboldt Fund.